



Hydrological Approach for Flood Overflow Estimation in Buleleng Watershed, Bali

R Suyarto¹, Wiyanti^{2*}, Moh Saifulloh¹, Anggia Widya Fatahillah², I Wayan Diara²,
Ketut Dharma Susila², Tati Budi Kusmiyarti²

¹ Spatial Data Infrastructure Development Center (PPIDS), Udayana University, Denpasar 80234, Indonesia

² Soil Science and Environment, Faculty of Agriculture Udayana University, Denpasar 80234, Indonesia

Corresponding Author Email: wiyanthi@unud.ac.id

<https://doi.org/10.18280/ijssse.130512>

ABSTRACT

Received: 16 February 2023

Revised: 17 March 2023

Accepted: 18 April 2023

Available online: 10 November 2023

Keywords:

Hydrology, peak discharge, river capacity, flood overflow, Buleleng Watershed

The Hydrology of a watershed, encapsulated within the biogeophysical characteristics of upstream, midstream, and downstream regions, governs the peak discharge. Notable flooding issues have been observed in the downstream region of the Buleleng Watershed, largely attributed to land use transitions from vegetative to built-up areas. This study seeks to delineate the flood overflow zone within the Buleleng River Basin, influenced by factors such as rainfall, land use, and soil texture. Data employed in this study encompass land use maps, an 8-meter resolution Digital Elevation Model, annual rainfall records, soil texture information, and river network maps. The adopted methodology involved field survey data collection, satellite image analysis, and hydrological approach computations. Peak discharge values for the Buleleng Watershed, derived for periods of 5, 10, 25, and 5-100 years, were determined to be 426334.44, 568445.88, 603035.31, and 617379 m³/s respectively, set against a river capacity of 312748.13 m³/s. Given the substantial overflow discharge from the Buleleng River, the watershed is susceptible to flooding. The study findings indicate a progressive annual increase in flood overflow predictions, necessitating targeted interventions such as drainage management, surface runoff control, and a review of spatial permits for settlement usage, particularly within watershed conservation areas.

1. INTRODUCTION

Floods present significant challenges globally, with particular prominence in numerous regions [1, 2], notably within tropical locales such as Indonesia [3, 4]. The susceptibility of Indonesia to floods is attributed primarily to its geographical positioning, which is exposed to extreme meteorological phenomena including intense rainfall and typhoons [5, 6]. Furthermore, the country's extensive river network, often subject to inadequate management, is liable to rapid overflow during heavy rainfall episodes [7, 8]. The ramifications of flood events in Indonesia are manifold and severe, encompassing loss of human life, extensive property and infrastructure damage, and substantial disruption to economic activities [9]. These effects are particularly pronounced in rural locales where the majority of inhabitants are dependent on agriculture and fishing for their livelihoods [10]. A recurrent cause of flood-related challenges is river overflow. This occurs when the river's capacity is overwhelmed by the volume of water it receives, leading to spillage beyond its banks.

River overflow flooding, a form of natural disaster, ensues when the water level in a river exceeds its banks, leading to the inundation of surrounding areas [11]. This type of flooding is notably prevalent in regions experiencing heavy rainfall or snowmelt, and where river systems have been subject to poor management. The aftermath of river overflow flooding can be extensive, damaging infrastructure, residential properties, and agricultural land, while also disrupting transportation and

commerce [12]. In densely populated urban settings, the consequences of river overflow flooding can be particularly catastrophic, with elevated risks of loss of life and significant property damage [13, 14]. To alleviate the impacts of such events, the implementation of effective flood management strategies is crucial. These may include the construction of levees and floodwalls, the development of early warning systems, and enhancements in land-use planning [15]. River overflow flooding poses a significant challenge to numerous global communities, necessitating proactive measures for its prevention and mitigation [16, 17]. Floods transpire when the discharge or volume of water coursing through a river or drainage channel surpasses its carrying capacity. Flooding is the result of water runoff exceeding the normal high water level, leading to an overflow from the riverbed and subsequent inundation of adjacent low-lying lands. Contributing factors to flooding encompass prolonged rainfall, soil erosion leading to rock exposure and reduced water absorption, waterway blockages due to improper waste management, illegal and unregulated logging, regional topology, and the conversion of land for settlement and office use [18, 19].

A watershed is delineated as an area confined by mountain ridges, wherein the rainwater that precipitates within this area is gathered by these ridges and is channeled through minor rivers to the principal river [20]. The hydrological state of a watershed can be substantially influenced by alterations in land use. Specifically, the transformation of land use from vegetation to built-up areas can escalate both peak discharge and surface runoff [21]. Such increases are attributed to a

decrease in water absorption capacity, and when this surpasses the river's capacity, the resultant runoff augments the potential for flooding [22, 23]. Peak discharge arises due to the amplification of surface runoff water, culminating in an increase in river water volume and subsequent flooding. Typically, peak discharge is influenced by two overarching factors: Rain and watershed characteristics. The former encompasses the quantity of rainfall, its intensity, duration, and distribution, while the latter includes the watershed area, its shape, topography, soil type, geology, and land use [24, 25].

To date, the academic literature has not featured publications estimating river overflow floods specifically within the province of Bali. Prior research has been conducted, with a focus on Jakarta, the capital city of Indonesia, in 2017 [26]. The research examined the damage resulting from river overflow floods utilizing a climate data approach, a case study centered on a specific river area was undertaken. The integration of field survey data with climate data was employed to estimate flood occurrences and associated damage in adjacent areas. It was posited that for larger river basin scales, this method may lack the necessary effectiveness. Consequently, it is argued that a hydrological approach incorporating geospatial data and river sampling surveys is requisite. The current study estimated river overflow floods, utilizing a scenario of projected rainfall for periods spanning 5 to 100 years, in conjunction with supplementary geospatial data. The study's output predominantly delivered estimates of river overflow floods in relation to river capacity. In this context, river capacity was assumed to be static, suggesting that if the estimates indicate high levels of rainfall up to 100 years into the future, river overflow floods will occur due to the volume of water surpassing the storage capacity.

The Regional Disaster Management Agency of Buleleng Regency has reported a substantial incidence of flooding in the area, with 191 cases documented from January to May in 2012. Data from the Public Works and Spatial Planning Office of Buleleng Regency, detailing the flood characteristics in Singaraja City over the past five years (2015-2019), are indicative of the flood patterns within this city. Specifically, the total area of the flood region has been calculated to be 17.39 ha, encompassing 2,789 ha, with an average flood height of 0.4 cm. The duration of flooding in Singaraja City varies between 1-4 hours, with a frequency of flooding that ranges from 2-7 times per year. Drainage issues in Singaraja City, such as unchecked land conversion, have contributed to an increase in surface runoff and heightened rates of erosion and canal sedimentation, thereby diminishing the capacity of the channel/drainage system. The lack of spatial data and future predictions of river overflow flooding motivated the conduct of this research. In this study, a hydrological approach and spatial analysis were employed to investigate overflow flooding. The primary objective of this research is to model inundation floods based on peak discharge values, river channel capacity, and estimated rainfall with return periods of 5, 10, 25, 50, and 100 years. This research is structured as follows: (1) Introduction, (2) Research methodology, which is divided into several subsections including research area, field sample, and data analysis, (3) Results and discussion, further divided into thematic map parameters, estimated rainfall and rainfall intensity, river capacity, and flood overflow estimations, (4) Discussion, and (5) Conclusions.

2. RESEARCH METHOD

2.1 Research area and field sample

Spatially, the Buleleng Watershed is located between 8°63'0.324"-8°14'14.712" South Latitude and 115°09'23.112"-115°04'55.416" East Longitude. Based on geographical location, the Buleleng Watershed is located in Sukasada District and Buleleng District, which Sawan District borders in the east, Banjar District in the west, and the Bali Sea in the north.

The case study is dominated by the use of forest land associated with dry land agriculture [27]. The most commonly found agricultural commodities in the field are horticultural crops such as mustard greens, carrots, chili peppers [28], flowering plants such as chrysanthemums [29] and other seasonal crops. The most common plantation commodities are cloves, coffee, and cocoa. The upstream area of this region boasts two tourist attractions in the form of Buyan and Tamblingan lakes [30], which are surrounded by agro-tourism activities [31], with strawberries as the flagship commodity [32]. The region is relatively fertile, with Andosol soil types prevalent in the upstream area. However, from a different perspective, other researchers have stated that the upstream area is at a high risk of landslides. This high potential for landslides is caused by the biophysical conditions of the area, including high rainfall, a slope inclination of over 45%, volcanic upper slope forms, and some upstream areas having sparse vegetation with dry fields as the primary land cover [33].

The Buleleng Watershed is a part of the Saba Daya Watershed SWP with an area of 3,359 ha and has an elongated headwaters shape. The Buleleng Watershed is located in two sub-districts, namely Sukasada District and Buleleng District, through nine villages and ten sub-districts, namely: Wanagiri Village, Gitgit, Sukasada, Nagasepeha, Petandakan, Sarimekar, Beratan, Liligundi, Banyuning Village, Singaraja Village, Tegal Banjar, Astina, Banjarjawa, Banjarbali, Kampung Kajanan, Kampung Baru, Kampung Bugis, and Kampung Anyar. The slopes in the Buleleng Watershed are flat (0-5%), wavy (5-10%), hilly (10-30%), and steep (>30%). The hilly slope class dominates the Buleleng Watershed with an area percentage of 32.93% of the watershed area. The broad slope of hilly and steep slopes results in higher surface runoff rates and volumes. In addition, land use in the Buleleng Watershed is dominated by plantations, which is 54.09% of the watershed area. Land use with low vegetation cover causes water to fall to the ground directly and accelerates the soil saturation point. Annual rainfall in the Buleleng Watershed is more excellent than 2,750 mm/year with a very high category which affects the peak discharge value and causes flooding in the Buleleng Watershed.

The field survey aims to check data obtained from maps with conditions in the field. The survey was carried out by measuring the width of the river and the height of the river body and documenting the location at each sampling point. Sampling points for morphometric measurements were carried out from upstream to downstream of the river. Samples 1 and 2 are located upstream, 3 to 5 are in the middle, and 6 to 12 are downstream. The sample point distribution map is shown in Figure 1.

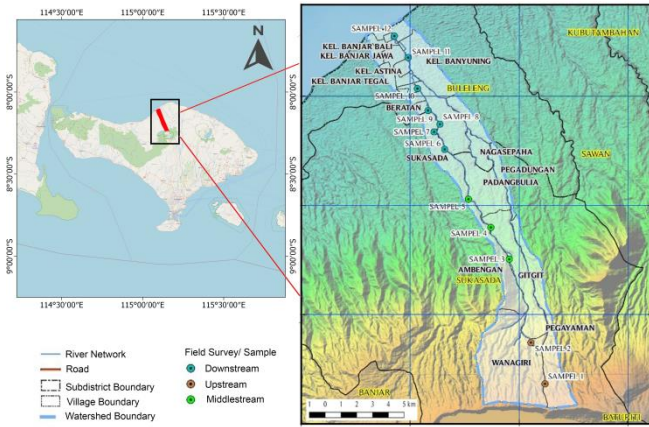


Figure 1. Research area and spatial distribution of field sample

2.2 Data analyst

Data analysis is a process of data into the latest information so that the data obtained becomes easier to understand and can be used to solve a research problem.

1. Calculation of peak discharge (rational method)

Calculation of peak discharge is carried out using the Rational method [34]. The parameters are surface runoff coefficient, rainfall intensity, and watershed area. The equation used is:

$$Qp = 0.278 \times C \times I \times A \quad (1)$$

where:

Qp: Peak discharge (m³/sec)

C: Surface runoff coefficient

I: Rain Intensity (mm/hour)

A: Watershed area (km²)

The amount of peak discharge is obtained through several stages, namely:

- The coefficient of surface runoff obtained from the overlay technique of slope maps, soil texture maps and land use maps using the method from [35].
- Rain intensity based on maximum rainfall data (R₂₄) and rain duration (t) [36]. Rain intensity is determined by the Mononobe equation, namely:

$$I = \frac{R_{24}}{24} \left(\frac{24}{t} \right)^{2/3} \quad (2)$$

where:

I: rainfall intensity (mm/hour)

R₂₄: maximum rainfall (mm)

t: rain duration (hours)

with the maximum daily rainfall in 24 hours (R₂₄) is determined using the equation:

$$R_{24} = \bar{X} + \frac{S_x}{S_n} (Y_t - Y_n) \quad (3)$$

where:

R₂₄: Maximum daily rainfall for 24 hours (mm/24 hours)

X: Average rainfall (mm)

Sx: Standard Deviation

Y_n: Reduced mean

S_n: Reduced standard deviation

Y_t: Reduced variation as return period

2. River capacity calculation

River capacity in the Buleleng Watershed was measured using the Manning method. River capacity describes the maximum discharge of a main river flow, which value is a threshold value to determine whether a peak discharge can cause flooding or not. The calculation of the maximum debit is calculated by the formula, namely:

$$Q = \frac{1}{n} \times A \times R^{2/3} \times S^{1/2} \quad (4)$$

where:

Q: Maximum discharge (m³/second)

A: Cross-sectional area of the river at the former flood (m)

R: Hydraulic radius of river cross section (m)

S: The hydraulic slope of the river water level when the maximum flood occurs by looking at the signs at the time of maximum flooding (%).

The amount of maximum discharge is obtained through several stages, namely the calculation of the cross-sectional area of the flooded river, hydraulic radius, wet perimeter, river bed width, hydraulic gradient and surface roughness coefficient shown in the Eq. (5).

- Calculation of the wet cross-sectional area using the Mean Section method, the width of one sub-section is determined by two adjacent vertical measurements (d_n and d_{n+1}). The width of the river is measured with a meter as shown in Figure 2, and the distance of each vertical section is measured by spatial analysis.

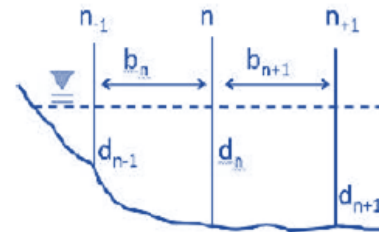


Figure 2. Sketch of river cross-sectional area measurement with mean section method

The cross-sectional area of the flooded river is calculated using the formula:

$$A = \left(\frac{d_1 + d_2}{2} \right) \times b_1 + \dots + [(d_n + d_{n+1}) \times (b_n)] \quad (5)$$

where:

A: Cross-sectional area (m²)

d: Depth of the riverbed from the maximum flood height (former flood/active flood) (m)

b: The length of the interval at the maximum cross section of the river

n: channel roughness value

- The hydraulic radius of the river has the following equation:

$$R = \frac{A}{P} \quad (6)$$

where:

R: Hydraulic radius (m)

A: Cross-sectional area of the river at the former flood (m²)

Q: Wet perimeter

c. The wet perimeter is determined by the equation:

$$P = b_0 + b_1 + b_2 + \dots + b_n + k \quad (7)$$

where:

P: Wet perimeter

b: The length of the interval at the maximum cross section of the river

k: The width of the river bed according to the cross section interval

$$S = \frac{H}{L} \quad (8)$$

where:

S: River hydraulic gradient

H: River level difference (m)

L: Length measurement

d. The surface roughness coefficient of the river channel whose magnitude is determined by the Manning roughness score based on Erena and Worku [37] and is calculated by the equation:

$$n = (n_0 + n_1 + n_2 + n_3 + n_4) \times n_5 \quad (9)$$

where:

n: Channel roughness value

n₀: Basic materials

n₁: Level of channel non-uniformity

n₂: Variation of channel cross section

n₃: The effect of narrowing in the cross section

n₄: Plants

n₅: Meander level

3. Determination of planned rain with Gumbel calculations

The design flood discharge is calculated based on the calculation of return period rainfall of 5, 10, 25, 50, 100 years. The data required is the average maximum rainfall obtained from the 2009-2018 rainfall data. The equation used for the planned rainfall is [36]:

$$X_t = \bar{X} + k \times S_x \quad (10)$$

where:

X_t: Rainfall estimation

\bar{X} : Average maximum rainfall

S_x: Standard deviation $\left(\sqrt{\frac{1}{n-1} \sum (X_1 - \bar{X})^2} \right)$

k: Frequency factor

3. RESULT

3.1 Thematic map parameters

The thematic maps presented in the first sub-chapter are slope, land use, and soil texture. The three maps' spatial analysis results are surface runoff maps. Classification of

slopes is flat (0%-5%), wavy (5%-10%), hilly (10%-30%), and steep (>30%), as indicated by surface runoff scores (10, 20, 30, and 40). The hilly slope class dominates the Buleleng Watershed with an area of 1,610.06 ha (47.93%), while the smallest area is the flat slope with an area of 403.25 ha (12%) which is located in the downstream part of the Buleleng Watershed (Figure 3(a)).

Soil texture maps are obtained through the interpolation process of soil sampling points. Based on the analysis results, four kinds of soil texture are loamy sand, sandy loam, loam, and loamy clay. Data regarding soil texture is needed to determine the infiltration capacity of the soil and the value of the surface runoff coefficient. Clay texture is the dominant soil texture in the Buleleng Watershed, with an area percentage of 46.37%, and clayey clay texture is the soil texture with the lowest percentage area, namely 7.54% (Figure 3(b)).

The results of land use digitization based on the 2018 SPOT 7 imagery show that there are four types of land use: Dense forest, mixed drylands, paddy fields, and settlements (Figure 3(c)). Land use influences the size of the influence on surface runoff, as shown by scores 5, 10, 15, and 20. Mixed dryland farming is the land use that dominates the Buleleng Watershed, which is 1816.92 ha with an area percentage of 54.09% of the watershed area. In comparison, the dense forest is a land use class with the smallest area of 56.84 ha, which is 1.69% of the watershed area.

The surface runoff coefficient is obtained through the overlapping process on the ArcGIS 10.4 application on slope maps, a soil texture map, and a land use map. Based on the results of the analysis that has been adjusted for the surface runoff coefficient score, four coefficient classes are obtained (low, normal, high, and extreme), as shown in Figure 3d. The slope, soil texture, and land use significantly affect the amount of water that becomes surface runoff. The results showed that the coefficient of surface runoff that dominates is a low class (0-25%) with an area of 1196.68 ha, while the normal class (25-50%) has the smallest area of 642.03 ha.

Rainfall data were obtained from the Bali Province BMKG at the Gitgit, Sukasada, and Wanagiri stations in 2009-2018. Based on the data processing and interpolation results using the isohyet, the rainfall class is less than 1,550 mm/year to more than 2,750 mm/year. The value of rainfall significantly affects the calculation of planned rainfall and rainfall intensity. Rainfall in the study area is >2,750 mm/year, with the highest percentage of 52.43% of the catchment area, while the class of 2,340-2,750 mm/year is the smallest area with a percentage of 4.52% of the catchment area (Figure 3(e)).

3.2 Estimated rainfall (X_t) and rainfall intensity (I)

Estimated rainfall can be estimated/calculated based on existing rainfall data. The analysis was carried out by planning future annual rainfall (Table 1). Estimated rainfall is calculated using average maximum rainfall (X_r), frequency factor (k), and standard deviation (S_x). The planned rainfall in the next 5 years is around 675.06 mm. In the next 10 years, it will be around 747.49 mm. In the next 25 years, it will be around 839.02 mm, and in the next 50 years, it will be around 906.91 mm. In the next 100 years, it will be around 974.31 mm. The rainfall intensity of the Buleleng Watershed is calculated based on rain thickness data (R₂₄) and duration of rain (t) for 24 hours and averaged from three stations Wanagiri, Sukasada, and Gitgit (Table 2).

Based on the results of data processing for 2009-2018 from

3 rain stations with a duration of 24 hours, rain intensity data for the 5 years were 122.91 mm/hour, the 10-year period was 125.93 mm/hour, the 25-year period was 129.74 mm/hour, 50 year period of 132.57 mm/hour, and 100 year period of 135.38 mm/hour.

Table 1. Rainfall estimations in Buleleng Watershed

Period (Year)	Maximum Rainfall (Xr)	Frequency Factor (K)	Standard Deviation (Sx)	Rainfall Estimation [Xt (mm)]
5	578.08	1.06	91.66	675.06
10	578.08	1.85	91.66	747.49
25	578.08	2.85	91.66	839.02
50	578.08	3.59	91.66	906.91
100	578.08	4.32	91.66	974.31

Table 2. Average rainfall intensity

Period (Year)	R ₂₄ (mm)	Rainfall Intensity (mm/hr)
5	2949.89	122.91
10	3022.33	125.93
25	3113.85	129.74
50	3181.75	132.57
100	3249.14	135.38

Calculating peak discharge using the rational method combines three parameters: The coefficient of surface runoff, rainfall intensity, and watershed area. The results of calculating the estimated peak discharge are presented in Table 3. Table 3 shows that the peak discharge in five years is

283,665.65 m³/second with an area of 936.48 ha. A period of 10 years of 426,334.41 m³/s with an area of 1,265.77 ha.

A period of 25 years of 452,276.48 m³/s with an area of 611.99 ha. A period of 50 years of 463,034.25 m³/s with an area of 601.82 ha. A period of 100 years of 473,680.03 m³/s with an area of 601.96 ha.

Table 3. Peak discharge (Qp) of the Buleleng Watershed

Period	Qp (m ³ /s)	Area (ha)	Percentage (%)
5	426334.43	936.48	27.88
10	568445.87	1265.77	37.68
25	603035.31	611.99	18.22
50	617379.20	601.82	17.92
100	631573.37	601.96	17.92
Area		3359.13	100

3.2 River capacity (Qmax)

The river capacity (maximum discharge) was obtained by the Manning method using the parameters of the channel roughness, cross-sectional area, hydraulic radius, and hydraulic slope of the river. Data for calculating river capacity in the Buleleng Watershed is carried out in the upstream, middle, and downstream parts of the river. The calculation results can be seen in Table 4.

The river capacity value in the upstream section is 294,546.94 m³/s, the middle is 18,138.65 m³/s, and downstream of 62.54 m³/s, so the total Q value is 312,748.13 m³/s. The maximum discharge value downstream is the smallest value when compared to other parts of the river.

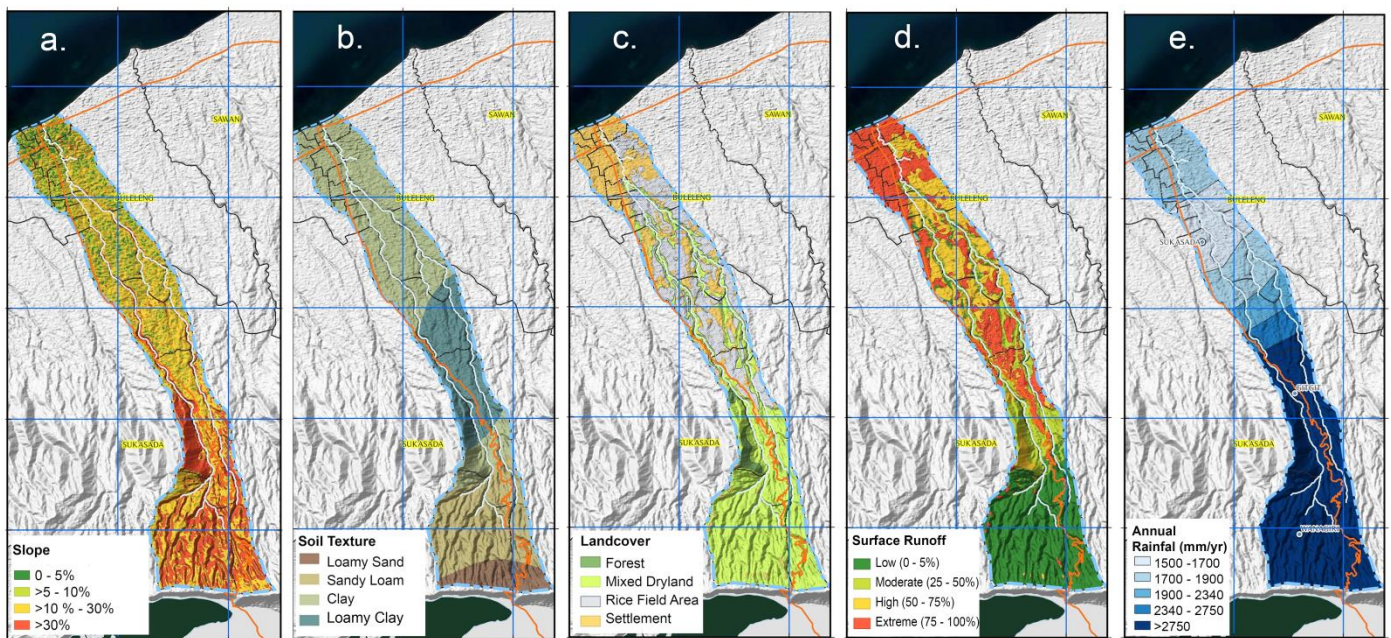


Figure 3. Spatial distribution of slope (a), Soil texture (b), Land covers (c), Surface runoff (d), and Annual rainfall (e)

Table 4. River capacity (Qmax)

No.	Watershed Area	Channel Roughness (n)	Cross-Sectional Area (m ²)	Hydraulic Network (R)	Hydraulic Tilt (S)	Qmax (m ³ /s)
1	Upstream	0.108	131202	0.50	0.15	294546.94
2	Middle stream	0.143	22957.33	0.33	0.05	18138.65
3	Downstream	0.155	232.14	0.14	0.02	62.54
Average			27741.75	Total		312748.13

3.3 Flood overflow estimation

Estimating flood overflow is obtained based on the difference between the peak discharge and the river's capacity. Estimated flood discharge for periods of 5, 10, 25, and 50-100 years are 113,586.31 m³/s, 255.697,74 m³/s, 290.287,18 m³/s, 304.630,87 m³/s, and 318.825,24 m³/s, respectively. The areas affected by flood overflows in 5, 10, 25, and 50-100 years are 470 ha, 603.31 ha, 734.14 ha, and 785.34 ha, respectively (Table 5).

Table 5. Flood overflow estimation

Period	Peak Discharge (Qp) (m ³ /s)	River Capacity (Qmaks) (m ³ /s)	Difference (Qp-Qmaks)	Area (ha)
5	426334.44	312748.13	113586.31	470.00
10	568445.88	312748.13	255697.74	603.31
25	603035.31	312748.13	290287.18	734.14
50	617379.00	312748.13	304630.87	785.34
100	631573.38	312748.13	318825.24	

Spatial distribution of flood overflows for 5 years, spread only in the river network area. The 10 to 25-year period is increasingly widespread in community settlements. The 50-100 year period spread throughout the downstream part of the Buleleng Watershed, which is spatially indicated by the maroon zone (Figure 4).

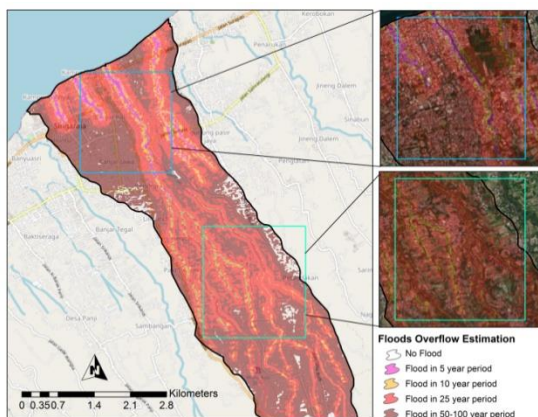


Figure 4. Spatial distribution of flood overflow estimation

4. DISCUSSION

The estimation of flood overflow is carried out in two stages, starting with the calculation of peak discharge estimation consisting of surface runoff coefficient (slope, soil texture, and land use), rainfall intensity, and watershed area. Furthermore, the river's capacity calculation is based on the parameters of surface roughness, depth, and hydraulic slope of the river. The results of the estimation of flood overflows spatially produce the area of affected villages with 5 periods, namely 5 years, 10 years, 25 years, and 50-100 years.

The surface runoff coefficient is a number that expresses the ratio between the amount of surface runoff to the amount of rainfall [38, 39]. The surface runoff coefficient with a low class (0-25%) covering an area of 1,196.68 ha is the dominating surface runoff in the Buleleng Watershed, spread in the upstream part of the Buleleng Watershed with slopes

from hilly (10-30%) to steep (>30%) (Figure 3(a)). Sandy loam texture and slightly loamy sand texture in the upper reaches of the watershed (Figure 3(b)). The dominant land use is mixed gardens, and the highest regional rainfall is around >2,750 mm/year (Figure 3(c)). The type of land use dramatically affects the value of surface runoff. Namely, the lower the vegetation cover, the higher the value of surface runoff.

Land use acts as a barrier and reduces surface runoff [40, 41]. Based on the research results that support the low surface runoff coefficient is the use of mixed garden land because surface runoff is restrained by rapid soil infiltration and canopies that reduce raindrops. The canopy has an impact on the rainfall intercept effect, which will weaken the impact of splashing raindrops on the soil surface and allow the soil to maintain a fast infiltration rate for a long time, thereby delaying the surface runoff time [42-44].

The surface runoff coefficient with medium class (25-50%) covering an area of 642.03 ha is the surface runoff with the smallest area in the Buleleng Watershed, and mixed gardens dominate land use with regional rainfall of 1,700-2,750 mm/year. The texture of loamy loam; and clay predominates in this area as well as wavy slopes (5-10%) to hilly (10-30%). The steep slope causes an increase in flow velocity, thus reducing the possibility of water penetrating the soil surface (infiltration) and water experiencing surface runoff. The flow pattern is affected by the slope, and the amount of surface runoff increases significantly due to the steeper slope compared to the gentle slope. Conversely, the smaller the slope, the greater the infiltration capacity, where the size of the runoff is affected by the infiltration capacity.

The high surface runoff coefficient class (50-75%) covering an area of 684.01 ha has wavy slopes (5-10%) with regional rainfall of 1,550-2,340 mm/year. The soil texture in this class is clay and has land use that is dominated by rice fields and settlements. Slow infiltration conditions that affect the high surface runoff, namely clay texture caused by rainwater reaching the soil surface, will fill the micro pores of the soil. Recent study by Holman-Dodds et al. [45] and Du et al. [46] states that soils dominated by the sand fraction will have macro pores, and soils dominated by dust will have many mesopores. At the same time, soils with a clay fraction will have many micro (small) pores, so the available water pore space consists of macro pore spaces. Moreover, some micropore spaces can bind water tightly so that it can inhibit the movement of water. Then it can be concluded that the finer the texture of the soil (clay), the higher the value of the surface runoff coefficient.

Extreme surface runoff coefficient (75-100%) covering an area of 836.41 ha has flat slopes (0-5%), hilly (5-10%), to hilly (10-30%) with land use dominated by settlements and rice fields. The scattered soil texture in this class is clay with an area rainfall of <1,550->2,750 mm/year. Land use, soil texture, and slope are closely related to rainfall intensity influencing surface runoff. Surface runoff occurs when the value of the rain intensity is greater than the infiltration capacity so that rainwater cannot infiltrate into the soil. In addition, the relationship between slope, soil texture (infiltration), land use, and rainfall intensity. The raindrops reaching the slope surface are prolonged with increased vegetation coverage. Soil infiltration time is also shortened, increasing runoff rate and runoff volume. The rain intensity is a source of surface runoff. The higher the rain intensity, the larger the average diameter of raindrops.

Surface runoff is very influential in the high peak discharge value. The parameters of slope and soil texture are static or do not change significantly within a certain period, while the parameters of land use are dynamic or easy to change. Changing land use conditions cause an increase in the peak discharge value for the period of 5 years to 10 years. Rain intensity could affect peak discharge, i.e., the more significant the intensity, the greater the peak discharge. The intensity of rain in the period of 25 years, 50 years to 100 years has increased, so the peak discharge value in that period will increase along with the increase in the value of the rain intensity. The increase in peak discharge due to rain intensity occurs because the flow of rainwater that is not infiltrated by the soil surface will directly flow into the flow system (rivers and lakes), and so the amount of peak discharge in the river also increases.

River capacity describes the peak discharge of a main river flow, which is the threshold value for determining whether peak discharge can cause flooding [47-49]. The calculation results of the peak discharge and river capacity show that the Buleleng Watershed cannot accommodate the peak discharge, so the Buleleng Watershed has the potential to flood. Buleleng Watershed, which has a high peak discharge, can be categorized as a watershed with a high potential for flood overflow. This is because the Buleleng Watershed has narrowed rivers, many river gradients, changes in land use, and higher rainfall intensity.

The area with the highest potential for flooding is the downstream part of the watershed. The overflow value increases due to the peak discharge value in each period and produces a different map of the affected area (Table 5). This is influenced by an increase in peak discharge to exceed the capacity of the river, and downstream, it is covered by buildings and paddy fields, which have a low infiltration value and causes higher surface runoff from the upstream part of the watershed. However, in the 50 and 100-year periods, there were no significant differences in spatial or calculation results, so the researchers combined flood overflow maps for the 50-100 year period (Figure 4). Peak discharge can cause flooding because the flow velocity is high enough, so we have to ensure that the value is constant at all times and can prevent flooding due to excess peak discharge and experiencing drought if peak discharge occurs. This research can be used as a basis for river management in the future. On the other hand, it is also a basis for mitigating floods and overflows, which can be implemented through long-term regional spatial planning regulations.

5. CONCLUSIONS

The estimated peak discharge in the Tukad Buleleng Watershed has increased each period. A quite drastic increase occurred from 5 years to 25 years, namely 426,334.44 m³/s to 603,035.31 m³/s with a river capacity of 312,748.13 m³/s. The difference in the value of difference between the peak discharge value and the capacity of the river is very high, so this indicates that the Buleleng Watershed has a high potential for overflow flooding. The planned rainfall has increased in each return period, from the 5 years of 669.35 mm to the 10 years of 817.69 mm. The total area affected by planned flood overflow for 5 years covering an area of 470 ha; 10 years covering an area of 603.31 ha; 25 years surrounding an area of 785.14 ha; period of 50 and 100 years covering an area of

785.34 ha. This research can be redeveloped using more complete parameters to estimate the planned flood overflow in more detail. Generally, research on flood estimation using hydrological approaches is rarely conducted in Indonesia. There has been a relatively similar study conducted in Jakarta, but with different estimation approaches and methods. Previous studies tend to use rainfall data as a flood estimation model, while our study uses rainfall data, coefficient runoff from thematic map data, and field measurements to obtain river channel capacity. The contribution of this study to future development is as a guide for managing river basins, normalizing river channels, and mitigating future flood disasters.

REFERENCES

- [1] Kakinuma, K., Puma, M.J., Hirabayashi, Y., Tanoue, M., Baptista, E.A., Kanae, S. (2020). Flood-induced population displacements in the world. *Environmental Research Letters*, 15(12): 124029. <https://doi.org/10.1088/1748-9326/abc586>
- [2] Arrighi, C. (2021). A global scale analysis of river flood risk of UNESCO world heritage sites. *Frontiers in Water*, 3. <https://doi.org/10.3389/frwa.2021.764459>
- [3] Yulianto, F., Suwarsono, Nugroho, U.C., Nugroho, N.P., Sunarmodo, W., Khomarudin, M.R. (2020). Spatial-temporal dynamics land use/land cover change and flood hazard mapping in the upstream Citarum watershed, West Java, Indonesia. *Quaestiones Geographicae*, 39(1): 125-146. <https://doi.org/10.2478/quageo-2020-0010>
- [4] Marfai, M.A., Sekaranom, A.B., Ward, P. (2015). Community responses and adaptation strategies toward flood hazard in Jakarta, Indonesia. *Natural Hazards*, 75: 1127-1144. <https://doi.org/10.1007/s11069-014-1365-3>
- [5] Musiyam, M., Jumadi, J., Wibowo, Y.A., Widiyatmoko, W., Nur Hafida, S.H. (2020). Analysis of flood-affected areas due to extreme weather in Pacitan, Indonesia. *International Journal of GEOMATE*, 19(75): 27-34. <https://doi.org/10.21660/2020.75.25688>
- [6] Priyambodoho, B.A., Kure, S., Yagi, R., Januriyadi, N.F. (2021). Flood inundation simulations based on GSMaP satellite rainfall data in Jakarta, Indonesia. *Progress in Earth and Planetary Science*, 8: 34. <https://doi.org/10.1186/s40645-021-00425-8>
- [7] Daksiya, V., Mandapaka, P.V., Lo, E.Y.M. (2021). Effect of climate change and urbanization on flood protection decision-making. *Journal of Flood Risk Management*, 14(1): e12681. <https://doi.org/10.1111/jfr3.12681>
- [8] Yamamoto, K., Sayama, T., Apip. (2021). Impact of climate change on flood inundation in a tropical river basin in Indonesia. *Progress in Earth and Planetary Science*, 8: 5. <https://doi.org/10.1186/s40645-020-00386-4>
- [9] Yulianto, F., Sofan, P., Zubaidah, A., Sukowati, K.A.D., Pasaribu, J.M., Khomarudin, M.R. (2015). Detecting areas affected by flood using multi-temporal ALOS PALSAR remotely sensed data in Karawang, West Java, Indonesia. *Natural Hazards*, 77: 959-985. <https://doi.org/10.1007/s11069-015-1633-x>
- [10] Emam, A.R., Mishra, B.K., Kumar, P., Masago, Y., Fukushi, K. (2016). Impact assessment of climate and land-use changes on flooding behavior in the upper

- Ciliwung river, Jakarta, Indonesia. *Water* (Switzerland), 8(12): 559. <https://doi.org/10.3390/w8120559>
- [11] Tanaka, T., Tachikawa, Y., Iachikawa, Y., Yorozu, K. (2017). Impact assessment of upstream flooding on extreme flood frequency analysis by incorporating a flood-inundation model for flood risk assessment. *Journal of Hydrology*, 554: 370-382. <https://doi.org/10.1016/j.jhydrol.2017.09.012>
- [12] Moncoulon, D., Labat, D., Ardon, J., Leblois, E., Onfroy, T., Poulard, C., Aji, S., Rémy, A., Quantin, A. (2014). Analysis of the French insurance market exposure to floods: A stochastic model combining river overflow and surface runoff. *Natural Hazards and Earth System Sciences*, 14(9): 2469–2485. <https://doi.org/10.5194/nhess-14-2469-2014>
- [13] Laudan, J., Zöllner, G., Thieken, A.H. (2020). Flash floods versus river floods—a comparison of psychological impacts and implications for precautionary behaviour. *Natural Hazards and Earth System Sciences*, 20(4): 999–1023. <https://doi.org/10.5194/nhess-20-999-2020>
- [14] Merz, B., Blöschl, G., Vorogushyn, S., Dottori, F., Aerts, J.C.J.H., Bates, P., Bertola, M., Kemter, M., Kreibich, H., Lall, U., Macdonald, E. (2021). Causes, impacts and patterns of disastrous river floods. *Nature Reviews Earth & Environment*, 2: 592-609. <https://doi.org/10.1038/s43017-021-00195-3>
- [15] Magliocchetti, M., Adinolfi, V., Viccione, G., Grimaldi, M., Fasolino, I. (2021). Small rivers and landscape NBS to mitigate flood risk. *Sustainable Mediterranean Construction*. <https://www.sustainablemediterraneanconstruction.eu/en/edizioni-speciali/si-2021-05/si-2021-05-032/>.
- [16] Syafri, R.R., Hadi, M.P., Suprayogi, S. (2020). Hydrodynamic modelling of Juwana river flooding using HEC-RAS 2D. *IOP Conference Series: Earth and Environmental Science*, 412: 012028. <https://doi.org/10.1088/1755-1315/412/1/012028>
- [17] Helmi, H., Basri, H., Sufardi, S., Helmi, H. (2019). Flood vulnerability level analysis as a hydrological disaster mitigation effort in Krueng Jreue Sub-Watershed, Aceh Besar, Indonesia. *Journal of Disaster Risk Studies*, 11(1): a737. <https://doi.org/10.4102/jamba.v11i1.737>
- [18] Maróti, M., Kusy, B., Simon, G., Lédeczi, Á. (2004). The flooding time synchronization protocol. In *SenSys '04: Proceedings of the 2nd International Conference on Embedded Networked Sensor Systems*, pp. 39-49. <https://doi.org/10.1145/1031495.1031501>
- [19] Hirabayashi, Y., Mahendran, R., Koirala, S., Konoshima, L., Yamazaki, D., Watanabe, S., Kim, H., Kanae, S. (2013). Global flood risk under climate change. *Nature Climate Change*, 3: 816-821. <https://doi.org/10.1038/nclimate1911>
- [20] Strahler, A.N. (1957). Quantitative analysis of watershed geomorphology. *Eos, Transactions American Geophysical Union*, 38(60): 913-920. <https://doi.org/10.1029/TR038i006p00913>
- [21] Daramola, J., Adepehin, E.J., Ekhwan, T.M., Choy, L.K., Mokhtar, J., Tabiti, T.S. (2022). Impacts of land-use change, associated land-use area and runoff on watershed sediment yield: Implications from the Kaduna Watershed. *Water* (Switzerland), 14(3): 325. <https://doi.org/10.3390/w14030325>
- [22] Kang, Y., Gao, J., Shao, H., Zhang, Y. (2020). Quantitative analysis of hydrological responses to climate variability and land-use change in the hilly-gully region of the loess plateau, China. *Water* (Switzerland), 12(1): 82. <https://doi.org/10.3390/w12010082>
- [23] Yulianto, F., Khomarudin, M.R., Hermawan, E., Nugroho, N.P., Chulafak, G.A., Nugroho, G., Udhi Catur Nugroho, Suwarsono, S., Fitriana, H.L., Priyanto, E. (2022). Spatial and temporal distribution of estimated surface runoff caused by land use/land cover changes in the upstream Citarum watershed, West Java, Indonesia. *Journal of Degraded and Mining Lands Management*, 9(2): 3293-3305. <https://doi.org/10.15243/jdmlm.2022.092.3293>
- [24] Cheah, R., Billa, L., Chan, A., Teo, F.Y., Pradhan, B., Alamri, A.M. (2019). Geospatial modelling of watershed peak flood discharge in Selangor, Malaysia. *Water* (Switzerland), 11(12): 2490. <https://doi.org/10.3390/w11122490>
- [25] Leopardi, M., Scorzini, A.R. (2015). Effects of wildfires on peak discharges in watersheds. *iForest - Biogeosciences and Forestry*, 8(3): 302-307. <https://doi.org/10.3832/ifer1120-007>
- [26] Wijayanti, P., Zhu, X., Hellegers, P., Budiyo, Y., van Ierland, E.C. (2017). Estimation of river flood damages in Jakarta, Indonesia. *Natural Hazards*, 86: 1059-1079. <https://doi.org/10.1007/s11069-016-2730-1>
- [27] Made, S.S., Made, A. (2021). Sustainable dryland management strategy in Buleleng Regency of Bali, Indonesia. *Journal of Dryland Agriculture*, 7(5): 88-95. <https://doi.org/10.5897/joda2020.0064>
- [28] Sastrawidana, I.D.K. (2019). Speciation of lead (Pb) and cadmium (Cd) in agricultural soil of Pancasari village as a vegetables central area of Bali, Indonesia. In *Proceedings of the 7th Mathematics, Science, and Computer Science Education International Seminar, MSCEIS 2019, Bandung, West Java, Indonesia*. <https://doi.org/10.4108/eai.12-10-2019.2296458>
- [29] Made Arjana, I.G., Situmeang, Y.P., Suaria, I.N. (2015). Study of development potential chrysanthemum in Buleleng regency. *International Journal on Advanced Science, Engineering and Information Technology*, 5(5): 350-354. <https://doi.org/10.18517/ijaseit.5.5.581>
- [30] Indriyani, N.M.P., Makalew, A.D.N. (2020). Ecotourism landscape planning in nature tourism park of Buyan - Tamblingan Lakes Tabanan and Buleleng Regency Bali province. *IOP Conference Series: Earth and Environmental Science*, 501: 012037. <https://doi.org/10.1088/1755-1315/501/1/012037>
- [31] Dewi, L.K.Y. (2014). Modeling the relationships between tourism sustainable factor in the traditional village of Pancasari. *Procedia - Social and Behavioral Sciences*, 135: 57-63. <https://doi.org/10.1016/j.sbspro.2014.07.325>
- [32] Febianti, F., Paramitha, M.W. (2022). Strawberry pick tourism marketing strategy in Pancasari Village, Sukasada, Buleleng. *Enrichment: Journal of Management*, 12(5): 4088-4094.
- [33] Diara, I.W., Suyarto, R., Saifulloh, M. (2022). Spatial distribution of landslide susceptibility in new road construction Mengwitani-Singaraja, Bali-Indonesia: Based on geospatial data. *International Journal of GEOMATE*, 23(96): 95-103.
- [34] Young, C.B., McEnroe, B.M., Rome, A.C. (2009). Empirical determination of rational method runoff coefficients. *Journal of Hydrologic Engineering*, 14(12):

- 1283-1289. [https://doi.org/10.1061/\(asce\)he.1943-5584.0000114](https://doi.org/10.1061/(asce)he.1943-5584.0000114)
- [35] Cook, H.L. (1946). The infiltration approach to the calculation of surface runoff. *Eos, Transactions American Geophysical Union*, 27(5): 726-747. <https://doi.org/10.1029/TR027i005p00726-2>
- [36] Koutsoyiannis, D., Kozonis, D., Manetas, A.A. (1998). mathematical framework for studying rainfall intensity-duration-frequency relationships. *Journal of Hydrology*, 206(1-2): 118-135. [https://doi.org/10.1016/S0022-1694\(98\)00097-3](https://doi.org/10.1016/S0022-1694(98)00097-3)
- [37] McCuen, R.H., Bondelid, T.R. (1981). Relation between curve number and runoff coefficient. *Journal of the Irrigation and Drainage Division*, 107(4). <https://doi.org/10.1061/jrcea4.0001425>
- [38] Erena, S.H., Worku, H. (2019). Dynamics of land use land cover and resulting surface runoff management for environmental flood hazard mitigation: The case of Dire Daw city, Ethiopia. *Journal of Hydrology: Regional Studies*, 22: 100598. <https://doi.org/10.1016/j.ejrh.2019.100598>
- [39] Dumedah, G., Andam-Akorful, S.A., Ampofo, S.T., Abugri, I. (2021). Characterizing urban morphology types for surface runoff estimation in the Oforikrom Municipality of Ghana. *Journal of Hydrology: Regional Studies*, 34: 100796. <https://doi.org/10.1016/j.ejrh.2021.100796>
- [40] Shrestha, S., Cui, S., Xu, L., Wang, L., Manandhar, B., Ding, S. (2021). Impact of land use change due to urbanization on surface runoff using GIS-based SCS-CN method: A case study of Xiamen city, China. *Land*, 10(8): 839. <https://doi.org/10.3390/land10080839>
- [41] Hu, S., Fan, Y., Zhang, T. (2020). Assessing the effect of land use change on surface runoff in a rapidly Urbanized City: A case study of the central area of Beijing. *Land*, 9(1): 17. <https://doi.org/10.3390/land9010017>
- [42] Guzha, A.C., Rufino, M.C., Okoth, S., Jacobs, S., Nóbrega, R.L.B. (2018). Impacts of land use and land cover change on surface runoff, discharge and low flows: Evidence from East Africa. *Journal of Hydrology: Regional Studies*, 15: 49-67. <https://doi.org/10.1016/j.ejrh.2017.11.005>
- [43] Mewded, M., Abebe, A., Tilahun, S., Agide, Z. (2021). Impact of land use and land cover change on the magnitude of surface runoff in the endorheic Hayk Lake basin, Ethiopia. *SN Applied Sciences*, 3: 742. <https://doi.org/10.1007/s42452-021-04725-y>
- [44] Das, P.C., Esraz-UI-Zannat, M. (2022). Assessing the impacts of land use-land cover changes on direct surface runoff: a remote sensing approach in Khulna City. *Water Science & Technology*, 85(10): 3122–3144. <https://doi.org/10.2166/wst.2022.097>
- [45] Holman-Dodds, J.K., Bradley, A.A., Potter, K.W. (2003). Evaluation of hydrologic benefits of infiltration based urban storm water management. *Journal of the American Water Resources Association*, 39(1): 205-215. <https://doi.org/10.1111/j.1752-1688.2003.tb01572.x>
- [46] Du, X., Jian, J., Du, C., Stewart, R.D. (2022). Conservation management decreases surface runoff and soil erosion. *International Soil and Water Conservation Research*, 10(2): 188-196. <https://doi.org/10.1016/j.iswcr.2021.08.001>
- [47] Klijn, F., Asselman, N., Wagenaar, D. (2018). Room for rivers: Risk reduction by enhancing the flood conveyance capacity of The Netherlands' large rivers. *Geosciences*, 8(6): 224. <https://doi.org/10.3390/geosciences8060224>
- [48] Jing, Z., An, W., Zhang, S., Xia, Z. (2020). Flood control ability of river-type reservoirs using stochastic flood simulation and dynamic capacity flood regulation. *Journal of Cleaner Production*, 257: 120809. <https://doi.org/10.1016/j.jclepro.2020.120809>
- [49] Bakker, M.H.N. (2009). Transboundary river floods and institutional capacity. *Journal of the American Water Resources Association*, 45(3): 553-566. <https://doi.org/10.1111/j.1752-1688.2009.00325.x>